

Multiferroic BaTiO₃-CoFe₂O₄ Nanostructures

H. Zheng,¹ J. Wang,¹ S. E. Lofland,³ Z. Ma,¹
 L. Mohaddes-Ardabili,¹ T. Zhao,¹ L. Salamanca-Riba,¹
 S. R. Shinde,² S. B. Ogale,² F. Bai,⁴ D. Viehland,⁴ Y. Jia,⁵
 D. G. Schlom,⁵ M. Wuttig,¹ A. Roytburd,¹ R. Ramesh^{1,2}

We report on the coupling between ferroelectric and magnetic order parameters in a nanostructured BaTiO₃-CoFe₂O₄ ferroelectromagnet. This facilitates the interconversion of energies stored in electric and magnetic fields and plays an important role in many devices, including transducers, field sensors, etc. Such nanostructures were deposited on single-crystal SrTiO₃ (001) substrates by pulsed laser deposition from a single Ba-Ti-Co-Fe-oxide target. The films are epitaxial in-plane as well as out-of-plane with self-assembled hexagonal arrays of CoFe₂O₄ nanopillars embedded in a BaTiO₃ matrix. The CoFe₂O₄ nanopillars have uniform size and average spacing of 20 to 30 nanometers. Temperature-dependent magnetic measurements illustrate the coupling between the two order parameters, which is manifested as a change in magnetization at the ferroelectric Curie temperature. Thermodynamic analyses show that the magnetoelastic coupling in such a nanostructure can be understood on the basis of the strong elastic interactions between the two phases.

Ferroelectromagnets, which display simultaneous magnetic and electric ordering, have recently stimulated much scientific and technological interest (1). The coexistence of magnetic and electric subsystems engenders the material with the “product” property (i.e., the composite exhibits responses that are not available in the individual component phases), thus allowing an additional degree of freedom in the design of actuators, transducers, and storage devices. However, the choice of single-phase materials exhibiting coexistence of strong ferro/ferrimagnetism and ferroelectricity is limited (2, 3). Van Suchtelen *et al.* proposed that composites of piezoelectric and magnetostrictive phases can be electromagnetically coupled via a stress mediation (4). Subsequent theoretical and experimental work has focused on bulk ceramics (5–8). In a film-on-substrate geometry, such composites can be created in two extreme forms. Figure 1, A and B, shows a “multilayer” geometry consisting of alternating layers of the ferroelectric phase (e.g., perovskite BaTiO₃) and the ferro/ferrimagnetic phase (e.g., spinel CoFe₂O₄). When the magnetoelastic coupling is purely through elastic interactions, the effect in a multilayer structure will be negligible due to the clamping effect of the substrate (9). Therefore, we focus our efforts on creating and analyzing a vertically aligned structure. Moshnyaga *et al.* (10) have used an approach that

creates three-dimensional nanoscale clusters of La-Ca-Mn-O (LCMO, perovskite) embedded in an insulating MgO (rocksalt structure) matrix. They have demonstrated the tuning of the transport properties of the LCMO nanoclusters through a mechanical coupling with the surrounding MgO regions. Figure 1, C and D, illustrates a heterostructure consisting of nanopillars of the ferro/ferrimagnetic phase embedded in a ferroelectric matrix. The intrinsic similarities in crystal chemistry (i.e., oxygen coordination chemistry) between the perovskite and spinel families lead to lattice dimensions that are compatible. For example, the perovskites have a lattice parameter of ~4 Å, which is generally within 5% of the basic building block of the spinels. Consequently, this presents the tantalizing possibility of heteroepitaxy in three dimensions (i.e., both in-plane as well as out-of-plane).

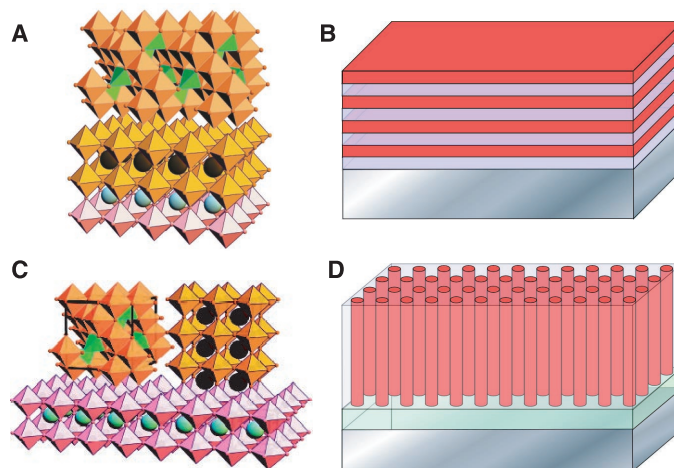


Fig. 1. (A) Superlattice of a spinel (top) and a perovskite (middle) on a perovskite substrate (bottom). (B) Schematic illustration of a multilayer structure on a substrate. (C) Epitaxial alignment of a spinel (top left) and a perovskite (top right) on a perovskite substrate (bottom). (D) Schematic illustration of a self-assembled nanostructured thin film formed on the substrate.

Thermodynamic analysis of such a structure has shown that the energy (e) of elastic interactions, including the direct interaction between the phases through elastic field in the film and the in-direct interaction through the substrate, can be given by (11–13):

$$e = G(S_1, S_2, \alpha)(\Delta\varepsilon)^2/2 \quad (1)$$

which depends on the compliance (S_1, S_2), the fraction [$\alpha, (1-\alpha)$] of the two phases, their relative configuration in the film (through the effective elastic modulus G), and the strain $\Delta\varepsilon$. Minimization of the overall elastic energy determines the equilibrium arrangements of the phases. For rodlike architectures (Fig. 1D), the main component of the elastic interaction energy due to the out-of-plane misfit ($\Delta\varepsilon_{\perp}$) is given by

$$e = (1/2)\alpha(1-\alpha)Y_1Y_2(\Delta\varepsilon_{\perp})/[(1-\alpha)Y_1 + \alpha Y_2] \quad (2)$$

where $Y = 1/S$ is the Young’s modulus. The elastic interactions, which dictate the morphological architecture of the phases in the film, simultaneously determine the coupling between order parameters in the phases. For a mixture of ferroelectric and ferro/ferrimagnetic phases

$$\Delta\varepsilon = \Delta\varepsilon_T + \varepsilon_0^P(P) + \varepsilon_0^M(M) \quad (3)$$

where $\varepsilon_0^P(P) = QP^2$ is the spontaneous ferroelectric strain, $\varepsilon_0^M(M)$ is the spontaneous magnetostriction, $\Delta\varepsilon_T$ is the misfit at deposition (modified by the difference in thermal expansion coefficients), and Q is the electrostriction coefficient. The connection between polarization (P) and magnetization (M) as well as $P(H)$ and $M(E)$ dependences can be obtained from the minimization of the free energy,

$$F = (1-\alpha)[\phi_P(P) - EP] + \alpha[\phi_M(M) - HM] + e[\varepsilon_0^P(P), \varepsilon_0^M(M)] \quad (4)$$

¹Department of Materials Science and Engineering, ²Department of Physics, University of Maryland, College Park, MD 20742, USA. ³Department of Physics, Rowan University, Glassboro, NJ 08028, USA. ⁴Department of Materials Science and Engineering, Virginia Tech, Blacksburg, VA 24061, USA. ⁵Department of Materials Science and Engineering, Pennsylvania State University, University Park, PA 16802, USA.

REPORTS

where ϕ_P (ϕ_M) is the specific free energy of uniform ferroelectrics (ferro/ferrimagnetics); H and E are magnetic and electric fields. It is clear from Eq. 4 that a strong magnetolectric coupling requires a strong interphase elastic interaction.

Self-assembled BaTiO_3 - CoFe_2O_4 nanocomposites were formed from a 0.65BaTiO_3 - $0.35\text{CoFe}_2\text{O}_4$ target by pulsed laser deposition. SrRuO_3 was chosen as the lattice-matched bottom electrode to enable heteroepitaxy as well as to facilitate electric measurements

(14). X-ray ($\theta - 2\theta$) scans reveal the high degree of crystallographic orientation in the nanostructure. In addition to the (00 l) peaks from the SrRuO_3 bottom electrode and the SrTiO_3 substrate, we observe only diffraction peaks that can be assigned to (00 l)-oriented spinel CoFe_2O_4 and perovskite BaTiO_3 , respectively (Fig. 2A). This suggests that the film has spontaneously separated into two phases during growth. Atomic force microscopy (AFM) images (Fig. 2B) show an interesting pattern that consists of a nearly

periodic microstructure, with hexagonal morphological features. Transmission electron microscopy (TEM) studies resolve these hexagonal patterns to be arrays of CoFe_2O_4 pillars with 20- to 30-nm diameters embedded in a BaTiO_3 matrix (Fig. 2C). We estimate a CoFe_2O_4 volume fraction of $\sim 35\%$ from such planar section images. Cross-section TEM reveals that the pillars go through the thickness of the film, and high-resolution images reveal the heteroepitaxy between the CoFe_2O_4 and the BaTiO_3 lattices. Plan-view electron diffraction patterns (Fig. 2D), together with cross-section diffraction patterns, resolve the orientation relationship: $[100] \text{SrTiO}_3 // [100] \text{SrRuO}_3 // [100] \text{BaTiO}_3 // [100] \text{CoFe}_2\text{O}_4$. On the basis of the x-ray diffraction, planar, and cross-section electron diffraction patterns, the three-dimensional (3D) lattice parameters were calculated ($\pm 0.005 \text{ \AA}$) to be $a = b = 3.99 \text{ \AA}$, $c = 4.04 \text{ \AA}$ for BaTiO_3 ; and $a = b = 8.38 \text{ \AA}$, $c = 8.31 \text{ \AA}$ for CoFe_2O_4 , indicating that CoFe_2O_4 nanopillars have a compressive out-of-plane strain of 0.8%. The change of (001) lattice parameter is due to the vertical heteroepitaxial mismatch between CoFe_2O_4 and BaTiO_3 .

Quasi-static ferroelectric measurements demonstrate well-defined ferroelectric hysteresis (Fig. 3A). The polarization values were normalized to the volume fraction of BaTiO_3 ($\sim 65\%$), yielding a saturation polarization (P_s) of $\sim 23 \mu\text{C}/\text{cm}^2$. Piezoelectric measurements reveal a clear hysteresis loop (Fig. 3B) with a maximum value of $\sim 50 \text{ pm}/\text{V}$ (as compared to the value of $\sim 130 \text{ pm}/\text{V}$ for single-crystal BaTiO_3). This decrease is primarily due to clamping effects from both substrate and the CoFe_2O_4 nanopillars (9). The decrease in d_{33} at high electric field is a consequence of the field-induced lattice hardening, which is typical of perovskite piezoelectrics. Dielectric measurements, carried out at 100 kHz, show a maximum dielectric constant of 330 to 350 (normalized to the volume fraction of BaTiO_3). Vertical-transport measurement yields a resistivity of $\sim 6 \times 10^9 \text{ ohm cm}$ at zero bias.

Superconducting quantum interference device magnetometry measurements (Fig. 3C) of the nanostructures show a saturation magnetization (M_s) of ~ 350 electromagnetic units/ cm^3 (normalized to the volume fraction of CoFe_2O_4 , $\sim 35\%$). The results show a strong anisotropy between the out-of-plane [001] and in-plane [100] directions. Linear extrapolation of the in-plane magnetization yields a uniaxial anisotropy field of $\sim 35 \text{ kOe}$. Calculation of the shape anisotropy (15) (based on the experimentally observed aspect ratio of ~ 10 and the measured saturation magnetization of $350 \text{ emu}/\text{cm}^3$) yields an anisotropy field of $H_{\text{shape}} \sim 2.1 \text{ kOe}$, which is significantly smaller than the experimentally observed value. Because no magne-

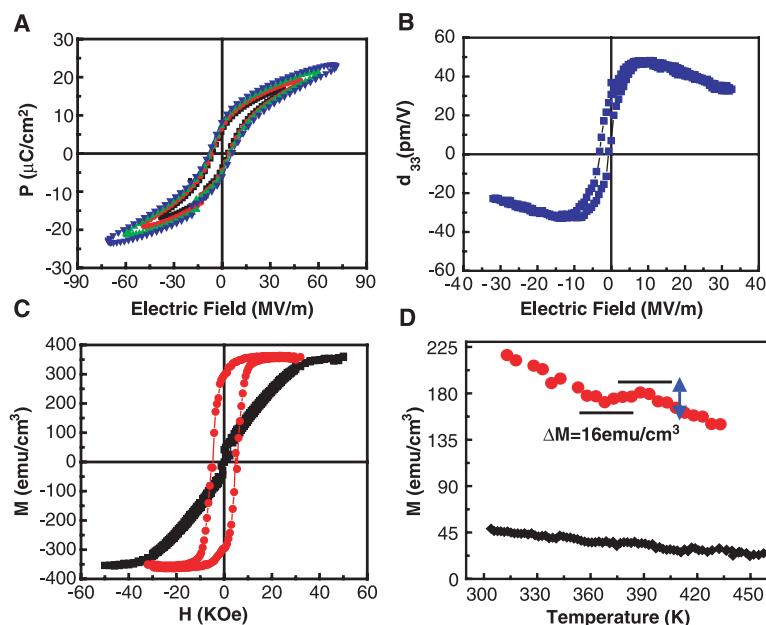
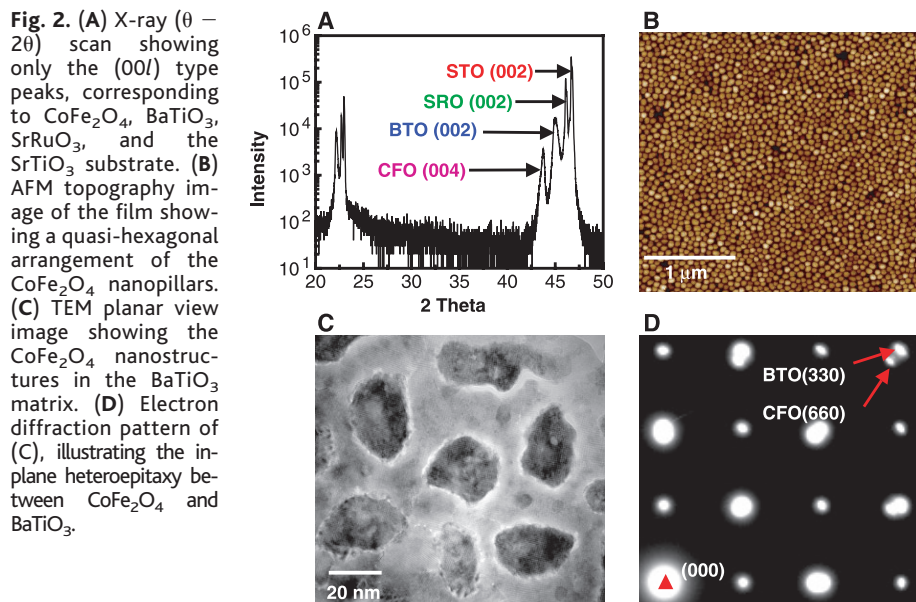


Fig. 3. (A) Polarization–electric field hysteresis loop showing that the film is ferroelectric with a saturation polarization $P_s \sim 23 \mu\text{C}/\text{cm}^2$. (B) Small-signal piezoelectric d_{33} hysteresis loop for a $50\text{-}\mu\text{m}$ -diameter capacitor. (C) Out-of-plane (red) and in-plane (black) magnetic hysteresis loops depicting the large uniaxial anisotropy. (D) Magnetization versus temperature curve measured at $H = 100 \text{ Oe}$, which shows a distinct drop in magnetization at the ferroelectric Curie temperature for the vertically self-assembled nanostructure (red curve); the multilayered nanostructure (black curve) shows negligible change in magnetization.

to crystalline anisotropy is expected between [001] and [100] directions for CoFe_2O_4 , the experimentally measured magnetic anisotropy should arise primarily from the magnetoelastic coupling. The first source of stress is the mismatch between the CoFe_2O_4 and BaTiO_3 lattices at the growth temperature ($\Delta\epsilon_T$). High-resolution TEM images (fig. S1) show that part of this mismatch is accommodated by the formation of interface dislocations. The second source of stress is the lattice distortion in the CoFe_2O_4 as a consequence of the cubic-tetragonal structural distortion in the BaTiO_3 matrix below the ferroelectric Curie temperature [$\epsilon_0^P(P)$]. This contribution decreases the compression along the axis of the CoFe_2O_4 nanopillar. This compressive strain in the CoFe_2O_4 lattice can be related to the magnetic anisotropy through its magnetostrictive effect. The stress in the CoFe_2O_4 is given by $\sigma_{001} = Y\epsilon_{001}$, in which Y is Young's modulus [~ 141.6 GPa (16)] and ϵ_{001} is the strain along the [001] direction. The magnetoelastic energy associated with it is $e = -3\lambda_{001}\sigma_{001}/2$, where λ_{001} is the magnetostriction coefficient of CoFe_2O_4 [taken to be $\lambda_{001} \sim -350 \times 10^{-6}$ (16)], leading to a magnetoelastic anisotropy energy of 5.95×10^6 erg/cm³. The anisotropy field is given by $H_{\text{stress}} = 2e/M_s = 34$ kOe, which is comparable to our experimentally observed value of ~ 35 kOe.

Results of temperature-dependent magnetization measurements (Fig. 3D, red curve) show coupling between the electric and magnetic order parameters in the self-assembled nanostructure. This is manifested as a distinct drop in the magnetization of ~ 16 emu/cm³ ($\sim 5\%$ of magnetization at a 100-Oe external field) around the ferroelectric Curie temperature ($T_c \sim 390$ K). At temperatures higher than T_c , the CoFe_2O_4 is compressed due to the lattice mismatch with BaTiO_3 . For $T < T_c$, the tetragonal distortion in the BaTiO_3 lattice decreases this compression in the CoFe_2O_4 . Because CoFe_2O_4 has a negative magnetostriction, it results in a reduction of the moment, as observed in our experiments. The change of magnetization near T_c can be estimated as $\Delta M/M \propto QP^2Y(d\lambda/dM)/M$ from a minimization of free energy (Eq. 4). However, quantitative estimation is difficult due to a lack of information about temperature dependence of $\lambda_{001}(M)$. For comparison, the temperature dependence of magnetization at 100 Oe (black curve in Fig. 3D) for a CoFe_2O_4 - BaTiO_3 multilayer sample with a layer thickness of ~ 30 nm shows negligible change around the ferroelectric Curie temperature. This can be understood as a consequence of the in-plane piezo-deformation in the multilayer structure being clamped by the substrate, thus precluding any deformation in the magnetic layer. This also proves that the coupling is dominated by elastic interactions in two-phase nanostructures.

In summary, an epitaxial CoFe_2O_4 - BaTiO_3 ferroelectromagnetic nanocomposite was made by a simple self-assembly technique. This system shows a strong coupling of the order parameters through the hetero-epitaxy of the two lattices. This approach is general—we have been able to create similar structures of other spinel-perovskite systems such as cobalt ferrite/bismuth ferrite and cobalt ferrite/lead titanate—and as such should impact a broad range of materials research.

References and Notes

1. N. A. Hill, *Annu. Rev. Mater. Res.* **32**, 1 (2002).
2. F. A. Smolenskii, I. E. Chupis, *Sov. Phys. Usp.* **25**, 475 (1982).
3. J. Wang *et al.*, *Science* **299**, 1719 (2003).
4. J. Van Suchtelen, *Philips Res. Rep.* **27**, 28 (1972).
5. R. E. Newnham, S. Trolier-McKinstry, *J. Appl. Crystallogr.* **23**, 447 (1990).
6. J. Van Den Boomgaard, A. M. J. G. van Run, J. Van Suchtelen, *Ferroelectrics* **14**, 727 (1976).
7. M. I. Bichurin, V. M. Petrov, Yu. V. Kiliba, G. Srinivasan, *Phys. Rev. B* **66**, 13404 (2002).
8. J. Ryu, S. Priya, K. Uchino, H. E. Kim, *J. Electroceramics* **8**, 107 (2002).

9. K. Lefki, G. J. M. Domans, *J. Appl. Phys.* **76**, 1764 (1994).
10. V. Moshnyaga *et al.*, *Nature Mater.* **2**, 247 (2003).
11. A. L. Roytburd, *Phys. Status Solidi A* **37**, 329 (1976).
12. A. L. Roytburd, *J. Appl. Phys.* **83**, 228 (1998).
13. A. G. Khachaturyan, *Theory of Structural Transformations in Solids* (Wiley, New York, 1993).
14. Materials and methods are available as supporting material on Science Online.
15. R. M. Bozorth, *Ferromagnetism* (IEEE Press, Piscataway, NJ, 1993).
16. V. J. Folen, in *Landolt-Börnstein*, vol. 3, part 4b, *Magnetic and Other Properties of Oxides and Related Compounds*, K.-H. Hellwege, A.M. Hellwege, Eds. (Springer, Berlin, Heidelberg, New York, 1970), pp. 366–393.
17. The work at the University of Maryland is supported by the NSF–Materials Research Science and Engineering Centers under contract DMR-00-80008, and Office of Naval Research–Multidisciplinary University Research Initiative under contract N000140110761. The work at Rowan University is supported by the New Jersey Commission on Higher Education.

Supporting Online Material

www.sciencemag.org/cgi/content/full/303/5658/661/DC1

Materials and Methods

Fig. S1

References

1 December 2003; accepted 22 December 2003

Crosstalk Between the EGFR and LIN-12/Notch Pathways in *C. elegans* Vulval Development

Andrew S. Yoo,^{1*} Carlos Bais,^{2*} Iva Greenwald^{2†}

The *Caenorhabditis elegans* vulva is an important paradigm for cell-cell interactions in animal development. The fates of six vulval precursor cells are patterned through the action of the epidermal growth factor receptor–mitogen-activated protein kinase (EGFR-MAPK) inductive signaling pathway, which specifies the 1° fate, and the LIN-12/Notch lateral signaling pathway, which specifies the 2° fate. Here, we provide evidence that the inductive signal is spatially graded and initially activates the EGFR-MAPK pathway in the prospective 2° cells. Subsequently, this effect is counteracted by the expression of multiple new negative regulators of the EGFR-MAPK pathway, under direct transcriptional control of the LIN-12–mediated lateral signal.

The six vulval precursor cells (VPCs) are consecutively numbered P3.p to P8.p (Fig. 1A). Each VPC has the potential to adopt one of three fates, termed 1°, 2°, or 3°. Descendants of the 1° and 2° cells constitute the vulva; the 3° cell daughters join the major hypodermal syncytium. Vulval development [reviewed in (1)] is initiated when LIN-3, an EGF-like signal produced by the gonad, activates the EGFR homolog LET-23 in the central VPC, P6.p. Activated LET-23, by means of a canonical Ras-MAPK cascade, causes P6.p to adopt the

1° fate and transcribe genes encoding the lateral signal (2). The lateral signal activates the receptor LIN-12/Notch in the two neighboring VPCs, P5.p and P7.p, causing them to adopt the 2° fate. Without activation of either the inductive or lateral signaling pathways, P3.p, P4.p, and P8.p adopt the 3° fate, believed to be as a result of inhibitory influences from the hypodermal syncytium.

Genetic and cell-ablation experiments have led to different models of inductive signaling (1). One model proposes that the inductive signal forms a morphogen gradient from the anchor cell, such that a high level of inductive signal causes the 1° fate, whereas a lower level helps specify the 2° fate (3). An alternative model proposes that VPC patterning is achieved by “sequential induction,” such that the inductive signal activates LET-23 only in P6.p, leading to a lateral signal that then induces P5.p and P7.p to adopt the 2°

¹Integrated Program in Cellular, Molecular, and Biophysical Studies, ²Department of Biochemistry and Molecular Biophysics, Howard Hughes Medical Institute, Columbia University, College of Physicians and Surgeons, 701 West 168th Street, Room 720, New York, NY 10032, USA.

*These authors contributed equally to this work.

†To whom correspondence should be addressed. E-mail: greenwald@cancercenter.columbia.edu